

# Suppression at High Spatial Frequencies in the Lateral Geniculate Nucleus of the Cat

M. J. Nolt, R. D. Kumbhani, and L. A. Palmer

*Department of Neuroscience, University of Pennsylvania School of Medicine, Philadelphia, Pennsylvania*

Submitted 25 September 2006; accepted in final form 24 June 2007

**Nolt MJ, Kumbhani RD, Palmer LA.** Suppression at high spatial frequencies in the lateral geniculate nucleus of the cat. *J Neurophysiol* 98: 1167–1180, 2007. First published June 27, 2007; doi:10.1152/jn.01019.2006. The spatial weighting functions of both retinal and lateral geniculate nucleus (LGN) X-cell receptive fields have been viewed as the difference of two Gaussians (DOG). We focus on a particular shortcoming of the DOG model, that is, suppression of responses of LGN cells at spatial frequencies above those to which the classical receptive field surround is responsive. By simultaneously recording one of the retinal ganglion cell (RGC) inputs (S-potentials) to an LGN cell, we find that half of this suppression at high spatial frequencies arises from the retinal input and that suppression in LGN cells is greater than that in RGCs, regardless of spatial frequency. We also inactivated the ipsilateral visual cortex and show that one quarter of the suppression at high spatial frequencies arises from corticothalamic feedback. We show that this suppression at high spatial frequencies is colocalized with the classical surround, is not dependent on the relative orientation of the center and surround stimuli, and that the cortical component of this suppression is divisive. We propose that the role of this suppression at high spatial frequencies is to restrict the response to large stimuli composed of high spatial frequencies.

## INTRODUCTION

Since the classic studies of Kuffler (1953) and Barlow (1953), the spatial weighting functions of both retinal and lateral geniculate nucleus (LGN) X-cell receptive fields have been viewed as the difference of two Gaussians (DOG) (Rodieck 1965). The DOG model consists of a strong and narrow central Gaussian and a weak but broad surround Gaussian. This linear model accounts for many properties of retinal ganglion cells (RGCs) and LGN cells, but numerous authors have described excitatory and/or suppressive effects in LGN cells that are not accounted for by the classic DOG model (Alitto and Usrey 2003; Cudeiro and Sillito 1996; Levick et al. 1972; Murphy and Sillito 1987; Solomon et al. 2002; Webb et al. 2002).

Many of these effects are attributed to a “nonclassical” receptive field and have proven to be controversial. Several authors have proposed that these effects are spatially localized to a region outside of the classical receptive field (e.g., Webb et al. 2002), although a recent study suggests that they are colocalized with the classical receptive field (Bonin et al. 2005). Sillito and colleagues described suppression in LGN cells that was dependent on the relative orientation of grating stimuli presented to the center and surround of the receptive field (Cudeiro and Sillito 1996; Sillito et al. 1993). They also

showed that the suppression found with isooriented, but not orthogonally oriented, stimuli was partially released on ablation of visual cortex. Others have failed to see these orientation effects in the intact animal (Bonin et al. 2005; Solomon et al. 2002; Webb et al. 2002) and Webb et al. (2002) reported no differential release of suppression after cortical ablation. Some studies have attributed changes in the gain of the classical receptive field to stimuli in the nonclassical surround. Webb et al. (2002) observed no effect of cortical inactivation on the gain of the receptive field, whereas others showed that cortical feedback may enhance responses in the LGN (Przybylszewski et al. 2000). Solomon et al. (2002) described a divisive reduction in response in the presence of an annular surround stimulus, but did not inactivate visual cortex.

In this report, we focus on a particular shortcoming of the DOG model: suppression of responses of LGN cells at spatial frequencies above those to which the classical receptive field surround is responsive. We examine spatial and functional properties of this suppression, including the controversial effects just described. We find that both the feedforward input from RGCs and feedback input from the ipsilateral visual cortex contribute to suppression at high spatial frequencies observed in the LGN and that suppression in the LGN is stronger than that in its retinal input regardless of the spatial frequency. We compare many of our findings with those of Solomon et al. (2002), who demonstrated suppression at the optimal spatial frequency of primate LGN cells and those of Bonin et al. (2005) who showed that the high spatial frequency cutoff of the suppressive field was 1.27-fold the cutoff value of the classical receptive field in cat LGN. We also discuss how our findings influence current receptive field models of LGN cells and how our results affect our understanding of the circuitry involved in the corticothalamic projection.

These conclusions are reached using two approaches. The first is to record simultaneously from LGN cells and one of their excitatory RGC inputs. This is accomplished by recording S-potentials, the extracellularly recorded postsynaptic signature of RGCs (Bishop et al. 1958; Cleland et al. 1971; Freygang 1958; Hubel and Wiesel 1961; Kaplan and Shapley 1984). Our second approach is to record extracellularly from LGN cells before, during, and after cooling of a large, retinotopically corresponding portion of visual cortex (areas 17 and 18). Some of these results have been presented in abstract form (Nolt et al. 2005).

Address for reprint requests and other correspondence: M. J. Nolt, University of Pennsylvania School of Medicine, Department of Neuroscience, 421 Curie Blvd., 1127 BRB II/III, Philadelphia, PA 19104 (E-mail: nolt@mail.med.upenn.edu).

The costs of publication of this article were defrayed in part by the payment of page charges. The article must therefore be hereby marked “advertisement” in accordance with 18 U.S.C. Section 1734 solely to indicate this fact.

## METHODS

*General*

Animals were prepared for single-unit recording as described in detail elsewhere (Nolt et al. 2004). Briefly, adult cats were anesthetized with 3–4% halothane in a 70:30 mixture of N<sub>2</sub>O and O<sub>2</sub>. Venous catheters were placed in each hind limb, gas anesthesia was discontinued, and the animal maintained on intravenous sodium thiopental as needed through the remainder of the surgery. A tracheotomy was performed, the animal was placed in a stereotaxic frame, and it was paralyzed with an injection of gallamine triethiodide (Flaxedil, 60 mg). The animal was maintained on positive-pressure ventilation adjusted so as to hold the end-expired CO<sub>2</sub> at 3.8%. Two venous catheters were used so that anesthetic (2–8 mg · kg<sup>-1</sup> · h<sup>-1</sup> thiopental) and paralytic (15 mg/h Flaxedil) could be infused throughout the experiment at independent rates. Cortical electroencephalogram (EEG) was monitored continuously throughout the experiment and the rate of anesthetic infusion regulated so as to maintain the animal in a state similar to light sleep characterized by frequent bursts of 7- to 10-Hz waves (spindles). Body temperature was also monitored and maintained at 38°C. A large craniotomy was made from Horsley–Clarke A11.0 to P10.0 and from the midline to L10.0 to allow access to the LGN and placement of the cooling plate over visual cortex. At the conclusion of the experiment, animals were given a lethal injection of sodium pentobarbital. This protocol was approved by the University of Pennsylvania's Institutional Animal Care and Use Committee and conforms to guidelines recommended in *Preparation and Maintenance of Higher Mammals During Neuroscience Experiments* (National Institutes of Health, publication 91–3207).

Neutral contact lenses were placed in each eye and spectacle lenses added to bring the reflection of retinal vessels into sharp focus on the screen of a CRT mounted in front of the cat. Biprisms were also placed in front of each eye to allow approximate superposition of the lines of sight, although cells were studied monocularly by covering the nondominant eye. Pupils were dilated with 1% ophthalmic atropine and the nictitating membranes retracted with 1% phenylephrine hydrochloride. Animals were given intramuscular (im) injections of glycopyrrolate (0.1 mg im once per day) to minimize secretions, dexamethasone (0.4 mg im once per day) to minimize cerebral edema, and ampicillin (10 mg/kg im) to prevent infection on a 12-h schedule. Most experiments lasted 1 day.

*Recording and data acquisition*

All recordings were made extracellularly with tungsten-in-glass electrodes. Signals were amplified and conditioned with a programmable amplifier (Alpha Omega, Nazareth, Israel). Amplified signals were routed to an oscilloscope, an audio monitor, and a spike sorter (Alpha Omega). The latter performed on-line template matching of action potentials and produced TTL pulses, which were detected at the computer interface during clock interrupt-service routines every 100 or 1,000  $\mu$ s, depending on the application. The electrode was advanced with a Burleigh Inchworm (Burleigh Instruments, Victor, NY). Penetrations were limited to layers A and A1 based on electrophysiological criteria; no histology was performed. All receptive fields were limited to the central 5° and within the 12.5° below the horizontal meridian of the visual field because this was the area of visual field covered by the cooling plate in visual cortex.

Visual stimuli were presented on an Image Systems multisynch monochrome monitor at a frame rate of 125 Hz by means of a VSG-2/3 board (Cambridge Research Systems, Cambridge, UK). Mean luminance was 80 cd/m<sup>2</sup> and lookup tables were linearized for contrasts in the range of  $\pm 100\%$ . The monitor was situated 24.7 cm from the eye such that 1 cm represents 2.3° of visual space. The screen subtended 36° horizontally and 27° vertically. Stimuli were presented with a resolution of 22 pixels/degree. An identical monitor driven in series was situated at the experimenter's console.

The responses of each cell were thoroughly characterized before any experimental procedures. This was accomplished in two phases. First, computer-assisted hand-plotting procedures were used to estimate the position and general properties of the receptive field in both the two-dimensional (2D) spatial and spatial-frequency domains (Jones and Palmer 1987). In the second stage, the parameters of the receptive field were refined using a series of programs, each of which generated stacks of histograms as stimuli spanning some variable were presented in random order. Specifically, we generated at least one spatial-frequency tuning curve and a contrast-response function for each cell. The temporal frequency of the stimuli ranged between 2 and 4 Hz. In addition, several procedures were used to ensure that the exact center coordinates of the receptive field were available for subsequent data acquisition. Along with the preliminary hand-plotting procedures, we used reverse correlation of the spike train with a dense, 2D spatiotemporal white noise stimulus (Reid et al. 1997). The position of the stimulus was modified until the most vigorous response elicited from the receptive field was centered within the stimulus. The centering of the stimulus was periodically reexamined because eye drift can cause shifts in the location of the receptive field. Changes in the receptive field location are often detected by changes in response phase, but this was rarely observed. Additional details will be described in RESULTS.

Details of our recordings of S-potentials have been described previously (Nolt et al. 2004). Using on-line template matching, we were able to simultaneously and independently extract both LGN and S-potential events.

Cells were classified as X and Y according to a set of standard criteria (Wolfe and Palmer 1998). For most cells, this included latencies to optic chiasm stimulation. Cells were also classified as lagged or nonlagged according to their responses to a spot covering both center and surround, which cycled between mean, bright, mean, and dark contrasts at 0.5 Hz (Saul and Humphrey 1990; Wolfe and Palmer 1998).

*Cortical cooling*

A silver-platinum plate was placed over a large portion of the visual cortex (areas 17 and 18), extending 5 mm down the medial bank, laterally 10 mm across the cortical surface, and from A2.0 to P9.0. The plate was cooled by a large Peltier device mounted on its superior surface. The other side of the Peltier device was cooled by water circulating through a water jacket. A microthermocouple (Omega Engineering) was inserted through a small hole in the plate to continuously monitor the temperature of the cortex. Temperature was measured at the tip of the probe, which was placed 2 mm from the surface, in layer VI of the cortex. For all of our experiments, we continuously recorded the temperature and cortical activity in layer VI.

Previous work shows that neuronal activity in cortex is abolished when the temperature reaches about 20°C (Lomber et al. 1999). We verified this by using extracellular recordings of multiunit activity. The orientation and spatial frequency selectivity of the activity were obtained before cooling of the cortex. Once layer VI was cooled to about 20°C, the activity ceased, but returned after warming of the cortex and retained its selectivity. In later experiments local field potentials and EEG were recorded in layer VI to monitor the cortical activity before, during, and after cooling (Fig. 1A). For all of our experiments, the temperature in layer VI was maintained between 15 and 20°C. After extended periods of cooling or after many cooling cycles, activity resembling seizures was often observed in the EEG. After cooling, if activity did not return to levels recorded before cooling or, if seizures were seen, the experiment was terminated.

To verify that cortical cooling does not affect the temperature of the LGN, we placed one microthermocouple in cortex and one in the LGN, and cooled layer VI of the cortex to about 20°C. Figure 1B

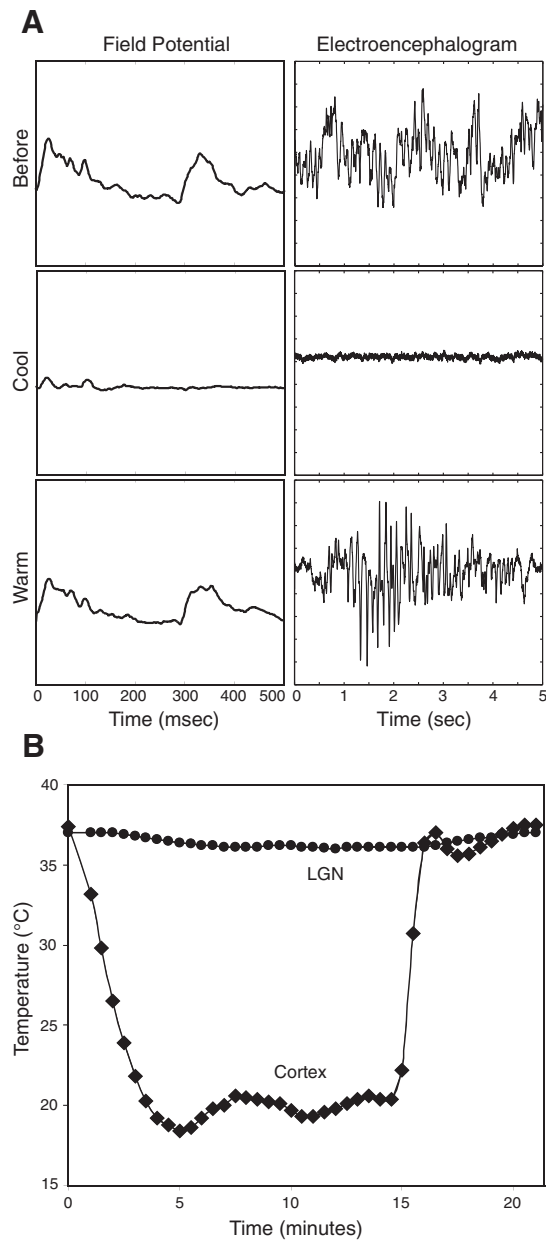


FIG. 1. Cortical activity and temperature before, during, and after cooling. *A*: visually evoked local field potentials (LFPs) and electroencephalogram (EEG) were recorded with electrodes placed in layer VI of visual cortex directly below the cooling plate. LFP and EEG were essentially flat when the visual cortex was cooled (*middle row*). *B*: temperature in the lateral geniculate nucleus (LGN) was not affected by cooling of the visual cortex.

shows that the temperature in the LGN remains constant throughout the cooling cycle.

RESULTS

We studied a total of 86 LGN X-cells in 29 male cats. Of these, 47 were associated with cooling of the ipsilateral visual cortex and 25 were associated with simultaneously recorded S-potentials. For 11 cells, the S-potential-LGN cell pair was held through at least one cortical cooling cycle. The length of time for which the cortex can be cooled is limited. As a result, for each cell or cell pair, data were available for a select number of the multipart protocols to be described below.

Suppression at high spatial frequencies

For each LGN cell, the analysis began by acquiring a spatial summation curve with contrast-modulated, spatially homogeneous disks (0 cycles/deg, DC) centered on the receptive field. The radius of the disk was varied in pseudorandom order. Each pass consisted of five cycles presented at each of 26 sizes and five to ten passes constituted a data set. There was no inter-stimulus interval but the first cycle for each size was discarded. An example for an X-cell in lamina A of the LGN is shown in Fig. 2*A*, where response amplitude (F1) is plotted versus the radius of the stimulus. As the stimulus increases in size, the response of the cell increases to a maximum. With further increases in radius, inhibition from the surround overtakes excitation from the center and the response decays reaching an asymptote at three to five times the radius at which the peak occurs.

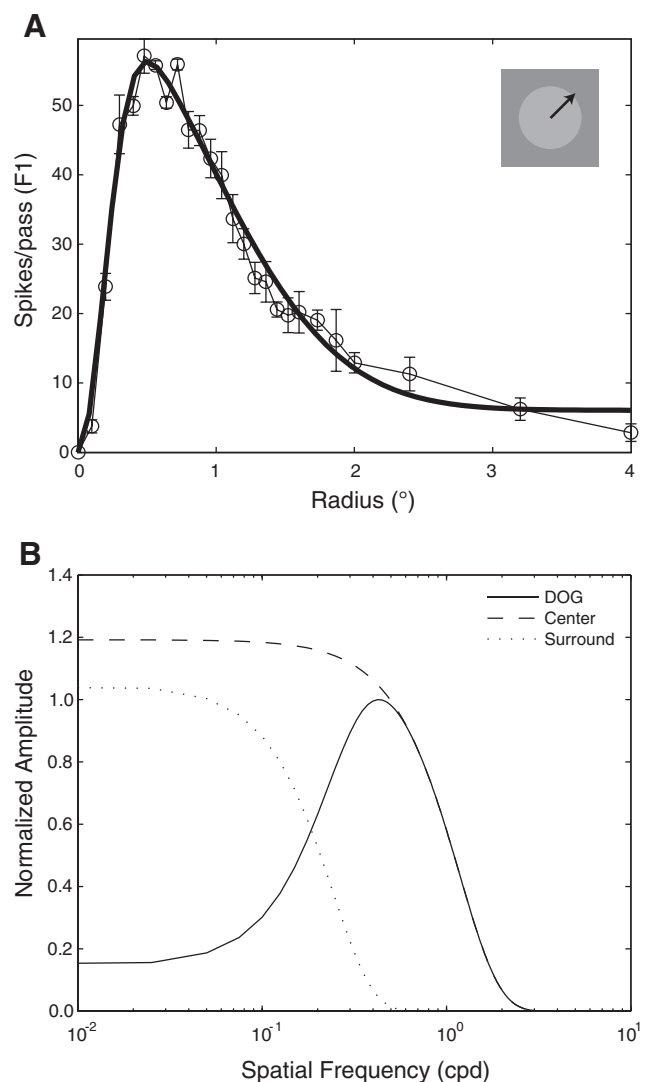


FIG. 2. *A*: spatial summation curve obtained with a spatially homogeneous disk (see *inset*) centered on the receptive field, whose luminance was modulated sinusoidally in time while its radius was varied in pseudorandom order. Spatial summation curve was fit with a 2-dimensional, polar integral of the difference of two Gaussians (solid line). *B*: assuming linearity of the receptive field, spatial frequency tuning curves of the center, surround, and their difference (DOG) were derived. Spatial frequencies above those to which the classical surround was responsive were chosen for further study.

We fit spatial summation curves to the 2D polar integral of the difference of two Gaussians (IDOG) with four free parameters

$$F(r) = 2\pi K_e \int_0^r r e^{-(r/R_e)^2} dr - 2\pi K_i \int_0^r r e^{-(r/R_i)^2} dr$$

where  $K_e$  and  $K_i$  are the strengths and  $R_e$  and  $R_i$  are the radii of the center and surround Gaussians, respectively. Fits were achieved with a simplex method modified from Press et al. (1988). Assuming linearity, we can then derive the spatial frequency tuning of the center, surround, and their difference as

$$R_c(f) = K_e \pi R_e^2 e^{-(\pi R_e f)^2}$$

$$R_s(f) = K_i \pi R_i^2 e^{-(\pi R_i f)^2}$$

$$R_{DOG}(f) = R_c(f) - R_s(f)$$

where  $R_c$ ,  $R_s$ , and  $R_{DOG}$  are the responses of the center, surround, and their difference, respectively, at the spatial frequency  $f$ . The spatial frequency tuning of the center, surround, and the DOG are shown in Fig. 2B for the example cell.

Spatial frequencies above those to which the surround is responsive, referred to here as “high spatial frequencies,” were selected for further examination. Spatial summation curves were obtained at high spatial frequencies by presenting drifting gratings centered on the receptive field with a background of mean luminance. The gratings drifted within a circular aperture whose radii were identical to those used with the homogeneous disk and were varied in pseudorandom order. A set of spatial summation curves obtained at high spatial frequencies is shown in Fig. 3A for the same cell as that shown in Fig. 2. Two key features of the set of curves in Fig. 3A are noteworthy: 1) the radius of the stimulus eliciting the peak response (“optimal size”) in the spatial summation curve decreased as the spatial frequency increased and 2) a strong reduction of the peak response was evident for large stimulus sizes at these high spatial frequencies. The response reduction in a given spatial summation curve was determined as

$$RR = 100 \left( 1 - \frac{R_{plateau}}{R_{peak}} \right)$$

where  $RR$  is the percentage response reduction of the peak response ( $R_{Peak}$ ) at the point where the response plateaus ( $R_{Plateau}$ ; see arrow in Fig. 3A). In Fig. 3, C and E, the optimal size of the spatial summation curve and response reduction are plotted versus normalized spatial frequency for our population of LGN cells ( $n = 20$ ). Spatial frequencies for each cell were normalized by the peak spatial frequency of the cell. Points representing the responses of individual cells are connected with line segments. It is clear that our population of LGN cells shows a decrease in the optimal size and an increase in the response reduction as the spatial frequency is increased.

Inhibition at low spatial frequencies can be accounted for by the classical surround, but this is clearly not the case for the response reduction at high spatial frequencies that we observe here. For example, in Fig. 3A, the spatial summation curve obtained with a drifting grating of 1.1 cpd reveals >50% response reduction even though the classical receptive field surround is tuned to spatial frequencies <0.5 cpd (Fig. 2B).

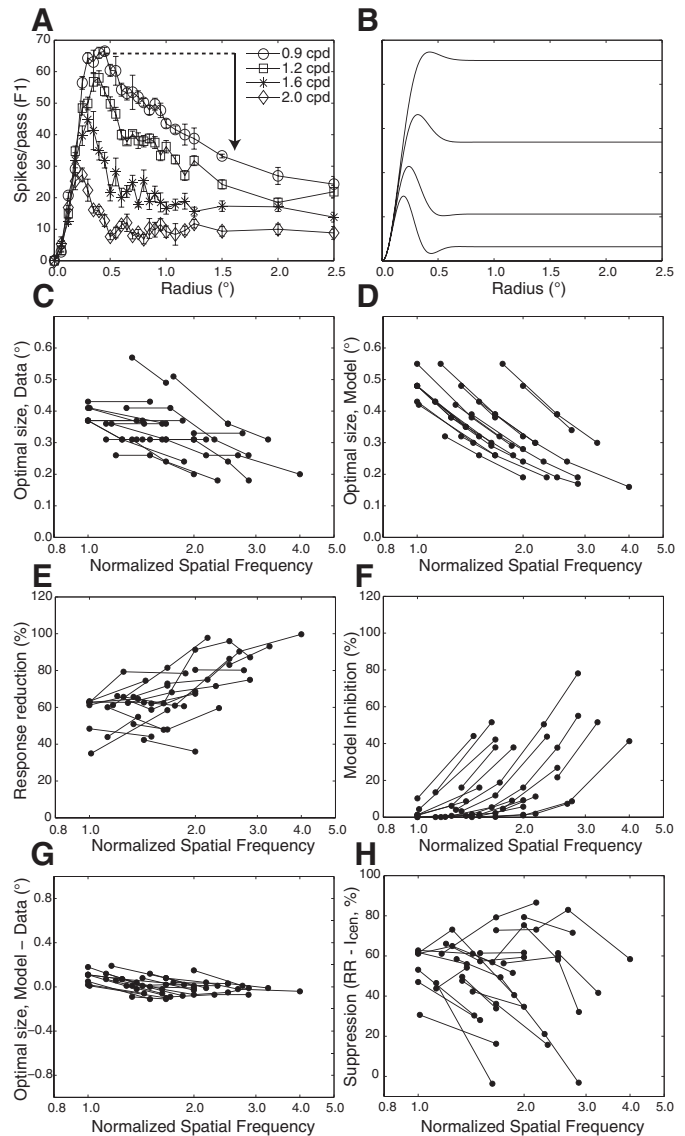


FIG. 3. Measured and computed spatial summation curves for LGN X-cells at high spatial frequencies. A: set of spatial summation curves for the LGN X-cell shown in Fig. 2, at spatial frequencies above those to which its classical surround was responsive. Optimal size decreases with increases in spatial frequency and response reduction is evident at high spatial frequencies (see arrow). B: set of computed spatial summation curves obtained by calculating the inner product of the center Gaussian spatial weighting function and the sinusoidal gratings used in A. As in the measured curves, the optimal size of the spatial summation curve decreases and the percentage inhibition increases with spatial frequency. C and D: optimal sizes of spatial summation curves obtained experimentally and computed using the model are plotted vs. normalized spatial frequency for 20 LGN cells. Points representing the responses of individual cells are connected with line segments. Nearly every cell shows a decrease in the optimal size as the spatial frequency is increased. E and F: response reduction calculated (see arrow in A) from the spatial summation curves obtained experimentally and the percentage inhibition computed using the model are plotted vs. normalized spatial frequency. Raw and modeled data show an increase in percentage response reduction and percentage inhibition, respectively, as spatial frequency is increased. G: difference in the optimal size obtained from the data and from the model is plotted vs. normalized spatial frequency. Optimal sizes in the data and the model are statistically indistinguishable ( $P > 0.05$ ). H: suppression is plotted vs. normalized spatial frequency.

### Contributions from the receptive field center

As the spatial frequency of the drifting grating increases, the optimal size of the spatial summation curve decreases slightly. This effect seems to follow from the linearity of the center mechanism alone. Having extracted the parameters of the best-fitting DOG, we computed expected spatial summation curves by calculating the inner products of the center Gaussian spatial weighting function and the sinusoidal gratings at those spatial frequencies tested in each cell. The grating was assumed to have even symmetry, i.e., it was a cosine centered on the classical receptive field and all spatial frequencies were at or above the optimal value for each cell.

Examples of the predicted spatial summation curves for the same LGN X-cell at high spatial frequencies are shown in Fig. 3*B*. Response amplitude is plotted versus the radius of the grating patch in both cases. For any radius, the response falls with spatial frequency because the spatial frequencies used are all above the optimal. The optimal size of the spatial summation curve decreases and the inhibition evoked by the center mechanism increases with spatial frequency in the predictions. Population data are plotted in Fig. 3, *D* and *E*. Both effects are a consequence of the linear behavior of the center mechanism: as spatial frequency increases, the patch size where half-cycles of the “wrong” polarity (dark in an ON-center cell, bright in an OFF-center cell) are presented to the center mechanism decreases and the recruitment of these “wrong” half-cycles produces inhibition. Therefore the response reduction is at least partly the result of inhibition from the linear behavior of the center mechanism. Note that adding the classical surround to the computation (not shown) has no effect on either the optimal size or the response reduction because all gratings were at spatial frequencies above those to which the classical surround responds.

Measured and computed results are compared for the population of LGN cells in Fig. 3, *G* and *H*. Computation of optimal size from the center mechanism agrees well with measured values (Fig. 3*G*,  $P > 0.05$ ,  $n = 20$ ). In general, the observed response reduction was more than could be accounted for by inhibition from the classical center mechanism alone (Fig. 3*H*). Here the response reduction not accounted for by the center mechanism in LGN cells is plotted versus normalized spatial frequency. This is a measure of the suppression that results from stimulating the nonlinear component of the receptive field with a high spatial frequency grating. We find that this suppression tends to decrease with spatial frequency. To determine the suppression elicited from the nonlinear component in spatial summation curves, we used the following suppression calculation

$$S = RR - I_{cen}$$

where  $S$  is suppression from the nonlinear component and  $I_{cen}$  is the inhibition expected from the center mechanism based on the assumption of linearity.

### Sources of suppression at high spatial frequencies

**RETINAL GANGLION CELLS (RGCs).** In principle, the suppression at high spatial frequencies could arise from at least three sources: the retinal input, processing intrinsic to the thalamus, or feedback from visual cortex. We examined the retinal input

by simultaneously recording LGN cells and S-potentials, the extracellularly recorded excitatory postsynaptic potentials resulting from the firing of RGC input to the relay cell (Bishop et al. 1958; Cleland et al. 1971; Freygang 1958; Hubel and Wiesel 1961; Kaplan and Shapley 1984). Recording S-potentials allows us to simultaneously examine the receptive field properties of an LGN cell and one of the RGCs providing its input. Because the RGC and LGN cell receptive fields are accurately superimposed (Hubel and Wiesel 1961; Nolt et al. 2004) and have the same spatial frequency tuning (So and Shapley 1981), we acquired spatial summation curves simultaneously for both cells using a single stimulus.

Figure 4*A* shows a set of spatial summation curves collected at high spatial frequencies for an RGC recorded simultaneously with the LGN cell in Figs. 2 and 3. In this example, the optimal size of the spatial summation curve decreased with spatial frequency and the response reduction increased with spatial frequency. These effects were also observed for our population data, shown in Fig. 4, *B* and *C*, where the optimal size of the spatial summation curve and response reduction are plotted versus normalized spatial frequency. We find that the population of RGCs exhibits the same behavior as the population of LGN cells: optimal size decreases and response reduction increases as the spatial frequency increases.

To determine the contributions of the center mechanism and the nonlinear component to the response reduction in RGCs, we used the same strategy as with LGN cells. We fit the DC spatial summation curve with an IDOG, extracted the parameters of the center Gaussian, and computed spatial summation curves with the center mechanism alone. We found that, just as with LGN cells, more response reduction was observed than could be accounted for by the inhibition from the classical center mechanism (Fig. 4*D*). Although in LGN cells suppression decreased with an increase in spatial frequency, in RGCs

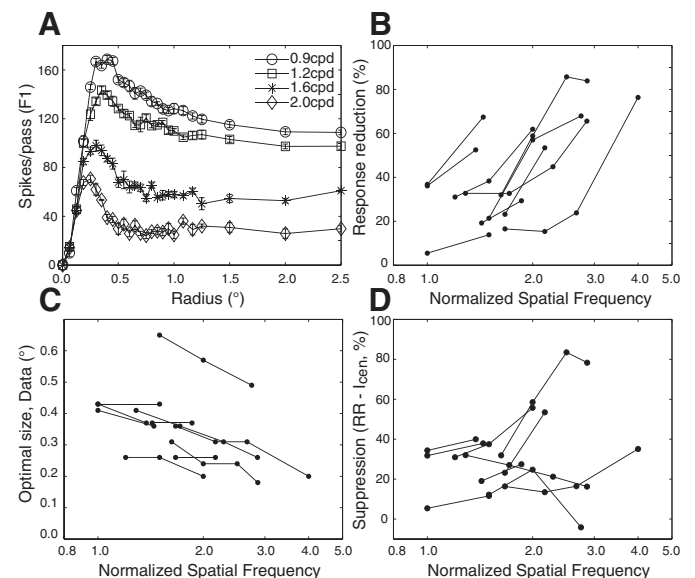


FIG. 4. *A*: spatial summation curves at high spatial frequencies for an X-retinal ganglion cell (RGC) simultaneously recorded with the LGN cell in Fig. 3. As shown for LGN cells in Fig. 3, response reduction increases (*B*) and optimal size decreases (*C*) with increases in spatial frequency for the population of RGCs ( $n = 10$ ). *D*: model does not account for the response reduction observed in spatial summation curves collected experimentally. See details for Fig. 3.

we find that suppression increases with spatial frequency for most cells. Importantly, these results show that at least some of the suppression at high spatial frequencies observed in LGN cells is already present in the RGC input.

To estimate the amount of suppression at high spatial frequencies that RGCs contribute to LGN cells, we quantified the suppression in simultaneously recorded RGC–LGN cell pairs as shown in Fig. 5. Data from 16 pairs are plotted in the *center panel*; each pair was examined at multiple spatial frequencies, with spatial frequency normalized by the optimal frequency for each cell (*x-axis*). It is evident that, with a few exceptions, more suppression was found in LGN cells than in their RGC inputs, regardless of spatial frequency. From the box and whisker plot at the *right* it can be seen that, on average, the suppression in LGN cells was almost twice that for the RGCs [RGC =  $29 \pm 3\%$  (SE); LGN =  $56 \pm 2\%$ ;  $P < 0.0001$ ]. These data suggest that about half of the suppression seen in LGN cells at high spatial frequencies arises from their individual RGC inputs. Inhibition evoked by spatially homogeneous (DC) stimuli in LGN cells was also about twice that seen in their RGC inputs (*left panel*, RGC =  $48 \pm 3\%$ ; LGN =  $89 \pm 2\%$ ;  $P < 0.0001$ ; Hubel and Wiesel 1961).

**VISUAL CORTEX.** To investigate the potential contribution of cortical feedback to suppression observed in LGN cells, we obtained spatial summation curves before, during, and after cooling of visual cortex. Figure 6A shows the results obtained for an LGN X-cell for both DC (*top row*) and high spatial frequency (*bottom row*) stimuli. It is evident from the *top row* that inhibition with a spatially homogeneous stimulus (DC) was unaffected by cooling of visual cortex. At a high spatial frequency (0.9 cpd, 1.13 times the optimal), however, response reduction with large patches of grating was significantly de-

creased when the cortex was cooled. The curve obtained in the precooled condition at high spatial frequency is replotted in gray in the *middle panel* of the *bottom row*. The response reduction for the largest three radii was significantly less ( $P < 0.05$ ) in the cooled versus the precooled state and recovered when the cortex was warmed.

This same difference was apparent in the population of 13 LGN X-cells for which at least one full cooling cycle was available for all 26 radii. Population data are plotted in Fig. 6B after normalization of both the response amplitude and the radii of the grating patches. Specifically, cortical cooling had no effect on the inhibition in the spatial summation curve obtained with homogeneous patches (DC, *top row*), but decreased the response reduction seen with high spatial frequencies (*bottom row*). As in Fig. 6A, the curve in the precooled condition at high spatial frequencies is replotted in gray in the *middle panel* of the *bottom row*. In these average data, the last 10 points differed significantly ( $P < 0.05$ ) between the cooled and both the precooled and postcooled conditions.

RGC data were also collected during the LGN cell recordings. Population data for RGCs and LGN cells are presented in Fig. 7 (6 RGC X-cells, 29 LGN X-cells). Inhibition before cooling is plotted versus inhibition during cooling for DC stimuli (Fig. 7, A and C) and suppression before cooling is plotted versus suppression during cooling for high spatial frequencies (Fig. 7, B and D). Not surprisingly, the RGCs do not show a significant difference in the amount of inhibition or suppression before versus during cooling for either the DC (Fig. 7A) or high spatial frequency (Fig. 7B) stimuli ( $P > 0.05$  for both). For the population of LGN cells, there is significantly less suppression at high spatial frequencies during cooling of the visual cortex (Fig. 7D,  $P < 0.01$ ), but

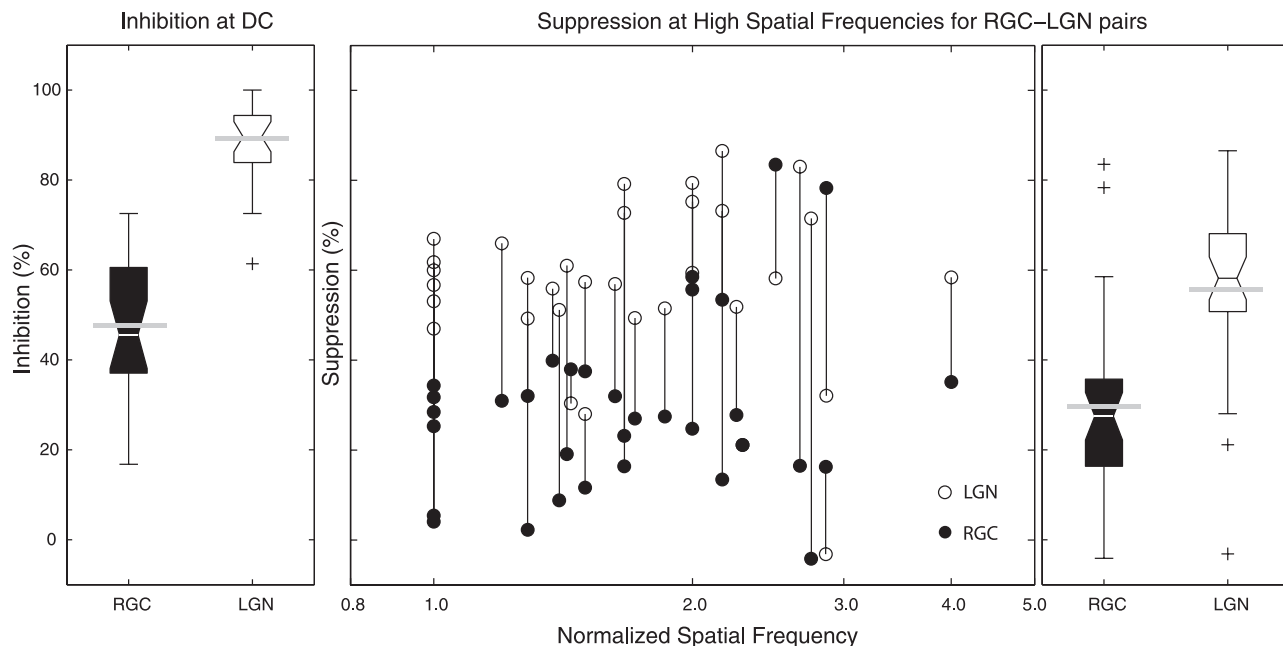


FIG. 5. Suppression and inhibition observed in simultaneously recorded RGC–LGN cell pairs. Box and whisker plot in the *left panel* shows that, on average, inhibition evoked by spatially homogeneous (DC) stimuli in LGN cells was about twice that of RGCs [RGC =  $48 \pm 3\%$ ; LGN =  $89 \pm 2\%$ ;  $P < 0.0001$ ]. In the *center and right panels*, suppression is plotted vs. spatial frequency for RGCs (●) and LGN (○) cells, with the members of each pair connected by a solid line. Spatial frequency was normalized by the optimal and results for each pair are plotted at multiple spatial frequencies. For almost every pair, suppression in the LGN cell is greater than that present in its RGC input, regardless of spatial frequency. Box and whisker plot in the *right panel* shows that, on average, the suppression evoked by high spatial frequency gratings in LGN cells was about twice that of RGCs [RGC =  $29 \pm 3\%$  (SE); LGN =  $56 \pm 2\%$ ;  $P < 0.0001$ ]. Gray horizontal lines show population means.

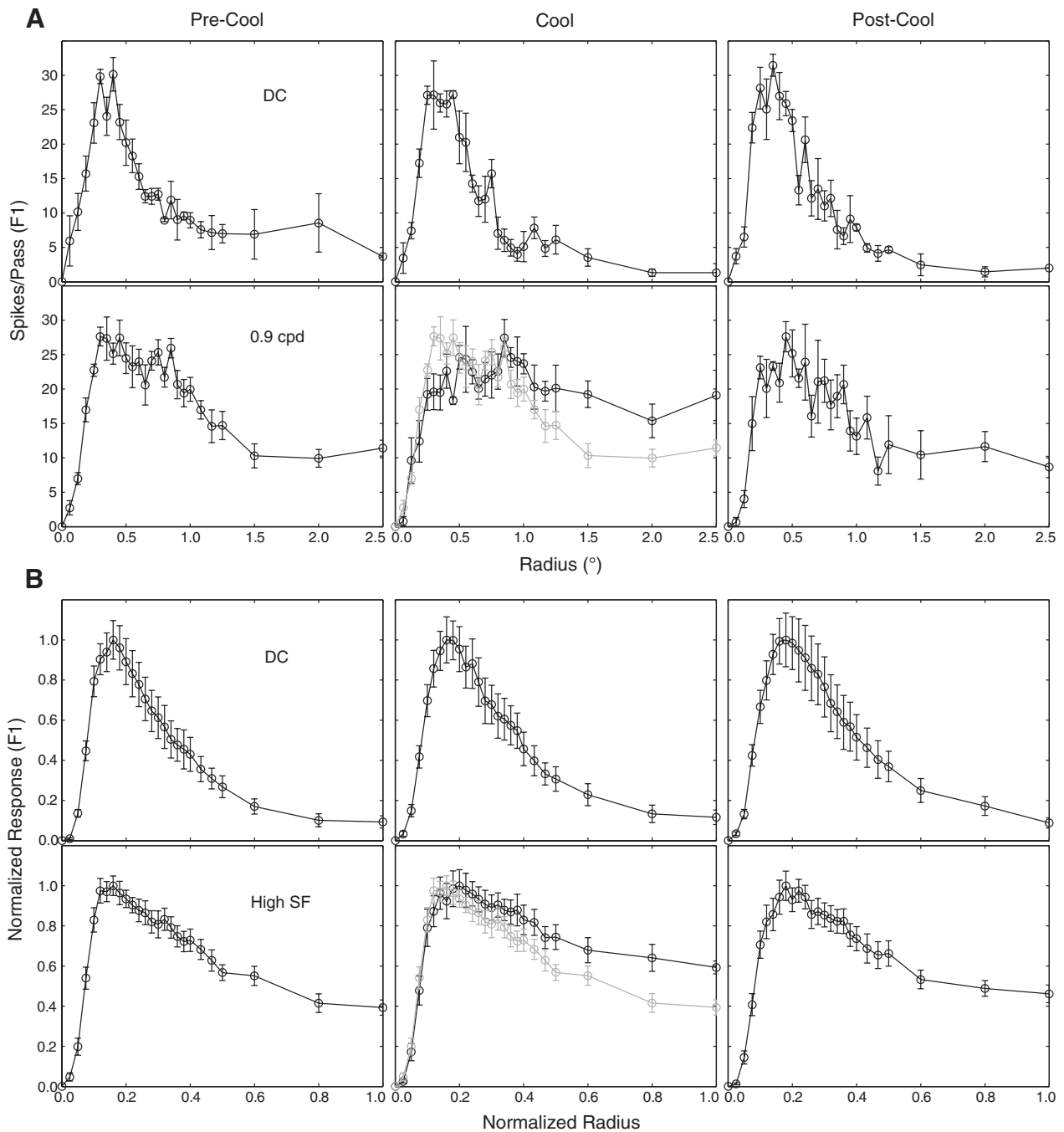


FIG. 6. Spatial summation curves before, during, and after cooling of visual cortex. *A*: spatial summation curves for an LGN X-cell for a spatially homogeneous (DC) stimulus (*top row*) and a high spatial frequency grating (*bottom row*). Inhibition evoked by the DC stimulus was unaffected by cortical cooling (*middle column*) but response reduction for the high spatial frequency grating was significantly decreased. For both *A* and *B*, the curve in the precooled condition at high spatial frequency is replotted in gray in the *middle panel* of the *bottom row*. *B*: spatial summation curves for the population of LGN X-cells for which at least one full cooling cycle was available for all 26 radii ( $n = 13$ ). Responses were normalized by the peak response for each cell. As in *A*, cortical cooling had no effect on the inhibition for the DC stimulus (*top row*), but significantly decreased the response reduction seen with high spatial frequency gratings (*bottom row*).

inhibition at DC is not affected (Fig. 7C,  $P > 0.05$ ). It is evident from the population data in Fig. 7 that cortical inactivation does not completely release the suppression observed at high spatial frequencies in LGN cells. We find that the cortical feedback is responsible, on average, for 27% of this suppression.

We conclude that both feedforward (RGC input) and feedback (from visual cortex) pathways contribute to suppression at

high spatial frequencies seen in LGN X-cells. Together, these two sources account for about three fourths of this suppression.

#### *Spatial extent of suppression at high spatial frequencies*

To determine the spatial locus of suppression at high spatial frequencies, we used a bipartite stimulus consisting of a small, central disk whose luminance was modulated sinusoidally in

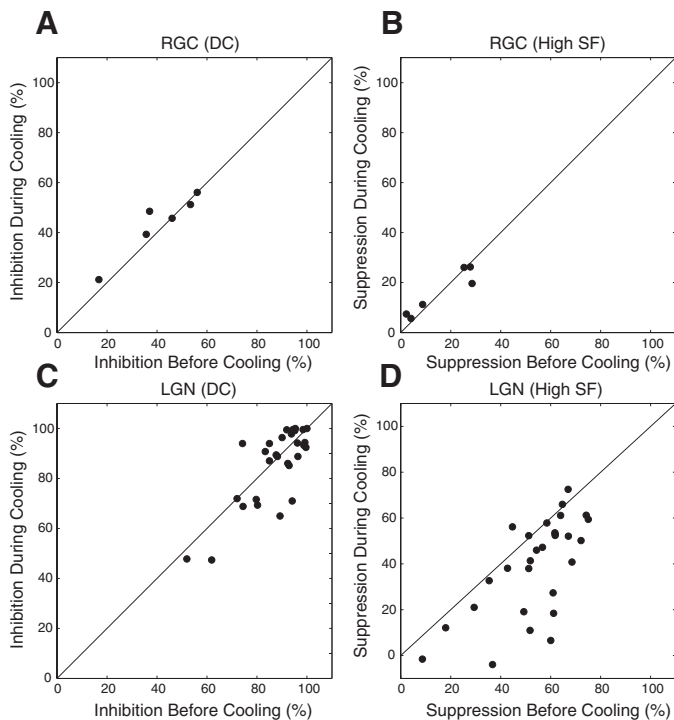


FIG. 7. Inhibition and suppression before and during cortical cooling for RGCs and LGN cells for spatially homogeneous (DC) stimuli and high spatial frequency gratings. Percentage inhibition or suppression during cooling is plotted vs. percentage inhibition or suppression before cooling. *A* and *B*: RGCs show no change in the amount of inhibition or suppression before vs. during cooling with either the DC or high spatial frequency stimuli ( $P > 0.05$  for both,  $n = 6$ ). *C*: LGN cells show no change in inhibition before vs. during cooling with DC stimuli ( $P > 0.05$ ,  $n = 29$ ). *D*: reduction in suppression is evident during cooling for high spatial frequency gratings ( $P < 0.01$ ).

time and a surrounding annulus whose outer diameter was fixed between 5 and 10°. This annulus contained either a high spatial frequency drifting grating or a uniform field and its inner diameter was varied in pseudorandom order, at 10 equally spaced steps. The center stimulus was fixed in size at the optimal size determined from the DC spatial summation curve and elicited a constant response (F1).

The high spatial frequency annuli suppressed the center response in a size-dependent manner as shown in Fig. 8. These data are pooled from 14 LGN X-cells. Responses are normalized on the y-axis by the response to the center alone, shown as the horizontal line at 1.0. The inner radii of the suppressive annuli were normalized by the outer radius used for each cell. The high spatial frequency stimuli evoked only nonlinear suppression because they did not encroach on the center of the receptive field. Compared with high spatial frequency gratings, inhibition evoked by spatially homogeneous annuli caused a greater reduction of the response elicited by the center stimulus. Inhibition by the spatially homogeneous annuli arises predominantly from the classical surround, although there is evidence suggesting they may also evoke suppression from the nonlinear component of the receptive field (Bonin et al. 2005). Importantly, the suppression evoked from the nonlinear component of the receptive field by high spatial frequency gratings declines over the same spatial range as the inhibition from DC stimuli. Therefore we conclude that the region evoking suppression at high spatial frequencies is precisely colocalized with the classical surround.

### Gain control

To explore potential effects of suppression at high spatial frequencies on the gain of the classical receptive field, we obtained contrast-response functions with gratings limited to the receptive field center (radius = optimal size) in the presence and absence of a high spatial frequency grating that filled the surrounding region as defined earlier. The contrast of the center grating varied between 0 and 64%, whereas the surround grating was fixed at 30%. These measurements were made before, during, and after cortical cooling.

The results are summarized in Fig. 9 for a population of 15 LGN X-cells. Responses were normalized to their peaks and averaged (Fig. 9A). The contrast-response function of the center alone (○) was unaffected by cortical cooling ( $P > 0.05$ ), and therefore the mean of the curves obtained before and during cooling is plotted for simplicity. On average, the high spatial frequency surround stimulus suppressed the response to the center stimulus by about half (◇), except at the highest contrast. Cooling of the ipsilateral visual cortex (\*) reduced the suppression at high spatial frequencies by about 30%. Because the center stimulus is the same in all cases, effects of the annuli arise from the action of the nonlinear component of the receptive field. On casual inspection, the curves seem to differ by a simple rotation about the origin, suggesting a divisive effect of the suppression at high spatial frequencies on the output of the neuron, also known as response gain control (Heeger 1992).

This idea was tested by fitting the curves with the hyperbolic ratio function

$$R(c) = R_{\max} \left( \frac{c^n}{\sigma^n + c^n} \right)$$

where  $R$  is the response at contrast  $c$ ,  $R_{\max}$  (unconstrained) is the maximum response, and  $\sigma$  is the semisaturation constant, or

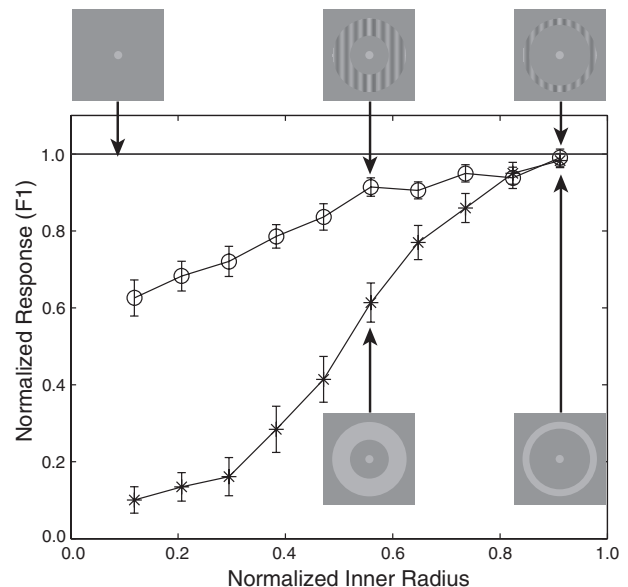


FIG. 8. Use of a bipartite stimulus to compare the spatial localization of the classical surround and the suppression observed with high spatial frequency gratings. High spatial frequency stimuli evoked only suppression from the nonlinear component of the receptive field. Responses of a population of 14 cells are normalized by their responses to the center stimulus alone (line at 1.0). Spatial distributions of the classical surround (\*, below) and the suppression at high spatial frequencies (○, above) are identical.

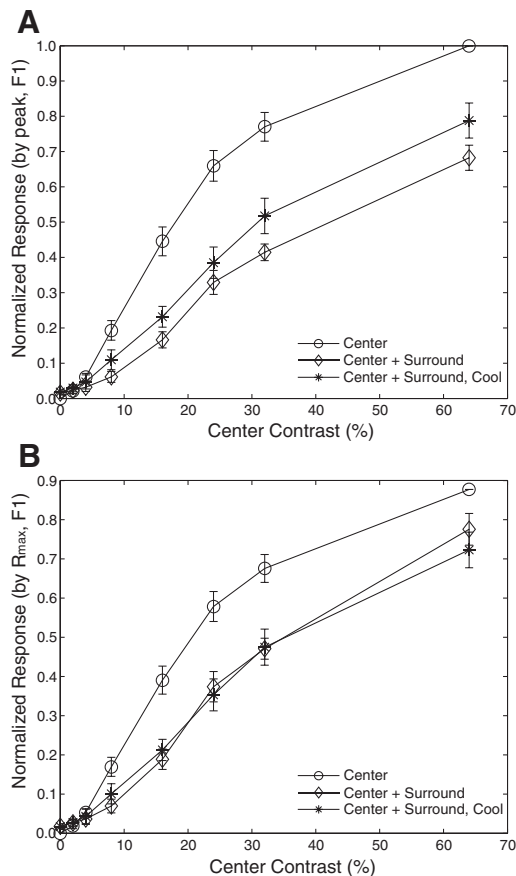


FIG. 9. Average contrast-response functions of 15 LGN X-cells obtained with a center stimulus in the presence and absence of a high spatial frequency grating in the surround before and during cortical cooling. Contrast of the surround stimulus was fixed at 30%. Because the center stimulus is the same in all cases, effects of the annuli are due to the action of the nonlinear component of the receptive field. *A*: normalized response ( $F1$ ) is plotted vs. percentage contrast for the center stimulus alone ( $\circ$ ) and for the center + surround stimulus before ( $\diamond$ ) and during ( $*$ ) cooling. The surround stimulus suppressed the response to the center stimulus by about 50%, and this suppression is reduced by about 30% during cooling. *B*: contrast-response functions in *A* were normalized by their respective  $R_{\max}$  values, obtained from fits to a hyperbolic ratio function. Contrast-response functions for the center + surround stimulus before ( $\diamond$ ) and during ( $*$ ) cooling are essentially identical, suggesting that the cortical component of the suppression functions only as a response gain control and not a contrast gain control.

the contrast at which the response of the cell is half of its derived maximum ( $R_{\max}$ ). If the nonlinear component of the receptive field was reducing only the  $R_{\max}$ , effectively dividing the output of the neuron, then the fitted curves should differ only in their  $R_{\max}$  values. In Fig. 9*B*, the three curves have been replotted after normalization by their respective  $R_{\max}$  values. The contrast-response function of the center alone ( $\circ$ ) differs significantly from the other two curves, suggesting that the overall effect of the suppression at high spatial frequencies is *not* simply a change in the  $R_{\max}$ , and is therefore not response gain control alone. Suppression at high spatial frequencies is likely a combined effect of response gain control and contrast gain control. However, the contrast-response functions for the center plus surround stimulus before ( $\diamond$ ) and during ( $*$ ) cooling are essentially identical after normalization by their respective  $R_{\max}$  values. Therefore these data suggest that the cortical component of

the suppression elicits a change in  $R_{\max}$  alone, functioning only as a response gain control.

#### Orientation tuning of suppression at high spatial frequencies

We examined the relative orientation dependence of the receptive field center and the surround at high spatial frequencies before and during inactivation of visual cortex. As shown in Fig. 10, we again used a bipartite stimulus to explore these issues. Both the center (at radius = optimal size) and surround stimuli were drifting, high spatial frequency gratings (Fig. 10*A*). The outer diameter of the surround stimulus was equal to the point where a plateau in the response was observed in the spatial summation curve and had either the same or orthogonal orientation relative to the center stimulus. The contrast of the surround was held constant at 30%, whereas the contrast of the center was varied between 0 and 64%, enabling us to obtain contrast-response functions for the center alone and for the center with both surround conditions.

Figure 10*B* shows the results obtained for an LGN X-cell. The average response amplitudes ( $F1$ ) to the center alone ( $\circ$ ),

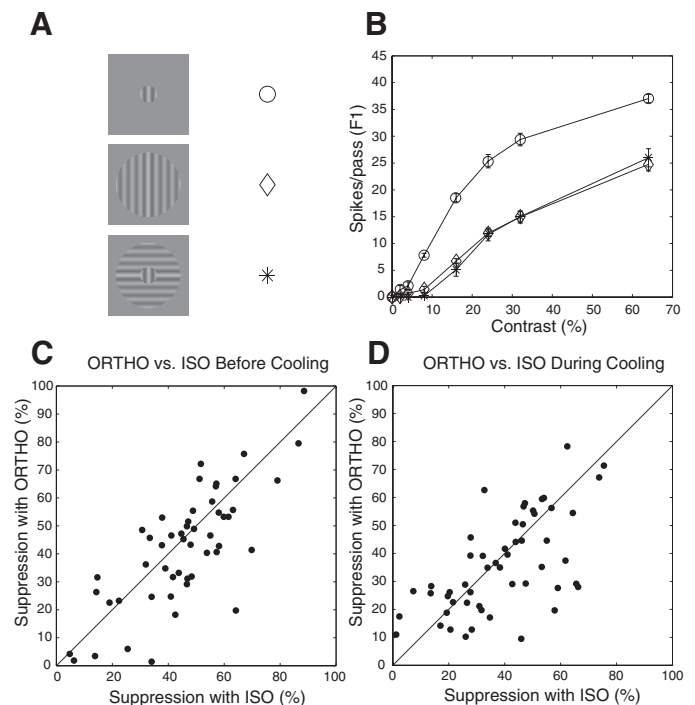


FIG. 10. Dependence of the suppression at high spatial frequencies on the relative orientation of the center and surround stimuli. Inhibition evoked by the center mechanism is not subtracted from the response reduction in the suppression calculation because its effect is constant across all conditions. Therefore any observed response reduction was evoked by suppression from the nonlinear component of the receptive field. *A*: stimuli: center stimulus alone, center stimulus with an iso- and orthogonally oriented surround stimulus. *B*: average response per pass for the three conditions, with response plotted vs. contrast of the center stimulus for an LGN X-cell. Contrast-response functions obtained with the two surround stimuli are nearly identical, showing that suppression is unmodified by the relative orientation of the center and surround stimuli, for all contrasts of the center stimulus. *C*: suppression observed with orthogonally oriented vs. iso-oriented surround for the population of 51 LGN X-cells, with the center at 32% contrast. *D*: data plotted as in *C*, for suppression observed during cortical cooling; 15 LGN X-cells are plotted at multiple center contrasts for each cell. Our population of LGN X-cells shows that suppression at high spatial frequencies is not dependent on the relative orientation of the center and surround stimuli, regardless of cortical state.

the center with the iso-oriented surround ( $\diamond$ ), and the center with the orthogonally oriented surround ( $*$ ) are plotted versus the center contrast. It is clear that the amount of suppression resulting from the two surround conditions is equivalent for all center contrasts. Suppression was calculated by comparing the response to the center stimulus alone with the response to the center stimulus with the appropriate surround condition. Inhibition evoked by the center mechanism is not subtracted from the response reduction in the suppression calculation because its effect is constant across all conditions. Therefore any observed response reduction was evoked by suppression from the nonlinear component of the receptive field. In Fig. 10C, orthogonally oriented suppression is plotted versus iso-oriented suppression for a population of 51 X-cells, with the center at 32% contrast. The points are grouped symmetrically about the line of unity ( $P > 0.05$ ), indicating that, as a population, suppression was unmodified by changes in the relative orientation of the center and surround at high spatial frequencies. The same result was obtained for other contrasts of the center stimulus (data not shown).

A similar result was obtained when the cortex was inactivated. This is shown in Fig. 10D, where the percentage suppression for iso-oriented and orthogonally oriented stimuli is compared during cortical cooling at multiple center contrasts for each cell. For the population, the two surround conditions show equal suppression ( $P > 0.05$ ,  $n = 15$ ). The iso- and orthogonally oriented stimuli show, on average across all center contrasts, 29 and 26% less suppression, respectively, compared with the suppression observed before cooling. The 3% difference between the two conditions is not statistically significant ( $P = 0.16$ ). This release of suppression (27.5%) during cortical cooling is numerically indistinguishable from that observed in the spatial summation experiment described earlier.

### Spatial frequency tuning curves

Given that the DOG model does not account for all of the response reduction at spatial frequencies greater than or equal to the optimal, the spatial frequency tuning curve of a cell should exhibit a lower peak and cutoff frequency than those derived from the DOG model. Spatial frequency tuning curves derived from IDOG fits to spatial summation curves obtained with DC stimuli were compared with those collected experimentally with drifting gratings. For each cell, the diameter of the drifting grating was at least equal to the diameter at which the response of the spatial summation curve reached a plateau. The two spatial frequency tuning curves for an example LGN X-cell are shown in Fig. 11A, normalized by their peak responses. In this example cell, both the peak and the cutoff frequencies of the measured curve are lower than those predicted from the IDOG fits. The cutoff is defined as the spatial frequency at which the tuning curve fell to half of the maximum response. Peak and cutoff frequencies for our population of cells are plotted in Fig. 11, B and C, with the measured values plotted versus the predicted values. In both figures, most points lie below the line of unity. For our population of cells, the peak and cutoff frequencies of the measured curves are significantly lower than those of the predicted curves ( $n = 28$ ; peak:  $P = 0.013$ ; cutoff:  $P = 0.002$ ).

We note that in the example cell in Fig. 11A, as in many of the cells, the responses at low spatial frequencies of the

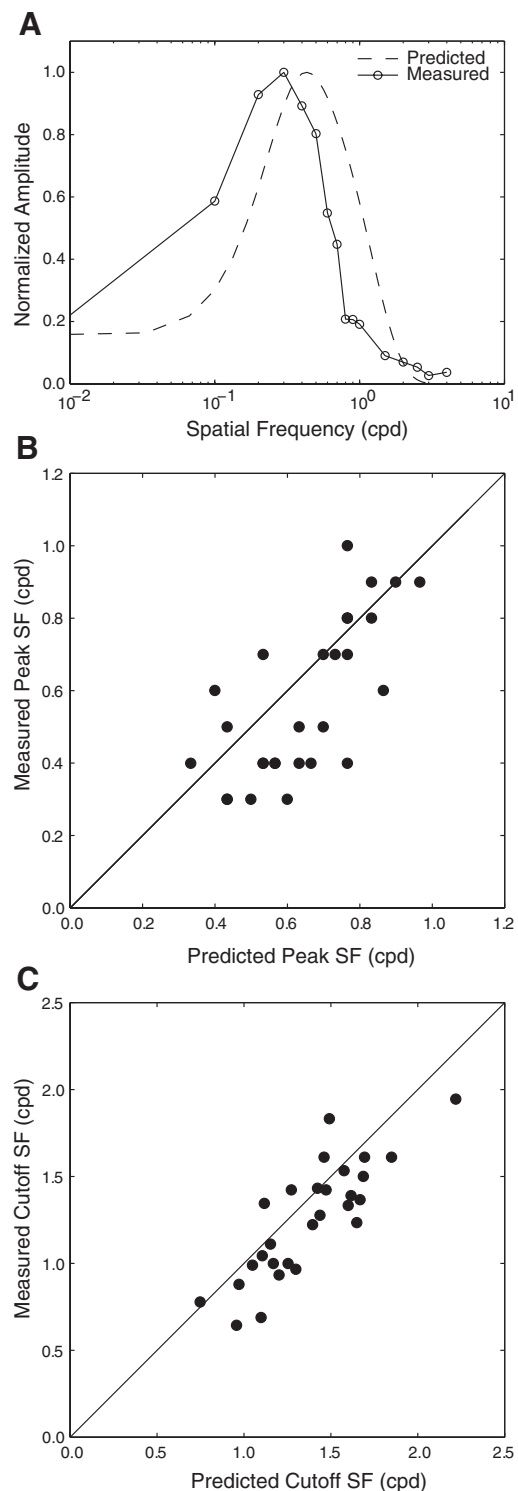


FIG. 11. Comparison of predicted and measured spatial frequency tuning curves. A: both spatial frequency tuning curves for an example cell, normalized by their peak responses. Peak and cutoff frequency for the measured (solid line) curve are lower than those derived from the spatial summation curve obtained with DC stimuli (dashed line). Peak (B) and cutoff (C) frequencies of the measured curves are plotted vs. the peak and cutoff frequencies of the predicted curves for our population of LGN X-cells ( $n = 28$ ). As a population, measured peaks and cutoffs are lower than predicted peaks and cutoffs (peak:  $P = 0.013$ ; cutoff:  $P = 0.002$ ).

predicted curve are lower than those of the measured curve. It appears that this is simply a result of the normalization. Because the responses at high spatial frequencies are suppressed in the measured curve, the peak frequency of that curve is shifted to lower values. After normalizing to the peak response, the responses at frequencies lower than optimal are artificially increased, giving the impression that these responses are higher than those in the predicted curve.

## DISCUSSION

We have shown that the responses of LGN X-cells are reduced by gratings whose spatial frequencies exceed those to which the classical surround is responsive. We focus on a component of this response reduction that is not accounted for by the classical DOG model of X-cell receptive fields. This nonlinear suppression is not orientation selective and is colocalized with the classical surround. It reduces the gain of the center in a complex manner and part of this reduction is the result of cortical feedback. About half of the suppression is already present in the retinal input, but it is augmented by a smaller component that is abolished during cortical inactivation.

### *Suppression at high spatial frequencies*

There is now a general consensus that the responses of LGN cells are suppressed by image components whose spectral composition extends well beyond that to which the classical surround is responsive. Using various methodologies, this has been demonstrated in the LGN for cat X-cells (Bonin et al. 2005); primate magnocellular, parvocellular, and koniocellular cells (Solomon et al. 2002); and most recently in primate magnocellular-projecting RGCs (Solomon et al. 2006). Using spatial summation curves collected at multiple spatial frequencies above those to which the classical surround is responsive, we show three effects are manifested as spatial frequency increases: 1) peak response diminishes, 2) the radius of the stimulus eliciting the peak response decreases, and 3) the fractional reduction of the peak response increases. The linearity of the center mechanism accounts for the shift in the optimal size, but the magnitude of the response reduction exceeds that which can be attributed to the inhibition from the center mechanism alone.

### *Comparison with RGC input*

All of the effects of high spatial frequency gratings apparent in LGN X-cells are also evident in their retinal inputs as identified by recording S-potentials (Bishop et al. 1958; Cleland et al. 1971; Freygang 1958; Hubel and Wiesel 1961; Kaplan and Shapley 1984) in conjunction with many of our LGN cells. However, the suppression at high spatial frequencies in RGCs is only about half that observed in their simultaneously recorded LGN cells. A similar result was obtained by Cleland et al. (1983) using moving bars of varying length. Our finding extends Hubel and Wiesel's original observation, that surround suppression is greater in the LGN than in the retina, to the entire range of spatial frequencies to which the cells respond.

We never saw more than a single S-potential in our simultaneous recordings. Thus we were not generally able to see all

of the retinal input to a given LGN cell. Nevertheless, greater suppression at high spatial frequencies was seen in LGN cells even though the efficacy of the single retinal input ranged widely (37–85%; data not shown). This suggests that each individual RGC that drives an LGN cell is equally suppressed and that suppressive effects do not add at the level of the postsynaptic LGN cell. Some of the remaining suppression at high spatial frequencies in LGN cells depends on input from visual cortex.

### *Cortical inactivation*

The effects of cortical feedback on the responses of LGN cells have been found to be excitatory (Baker and Malpeli 1977; Funke et al. 1996; Hull 1968; Kalil and Chase 1970; Przybyszewski et al. 2000), inhibitory (Cudeiro and Sillito 1996; Murphy and Sillito 1987; Sillito et al. 1993; Waleszczyk et al. 2005; Webb et al. 2002), or both (Marrocco et al. 1996; Waleszczyk et al. 2005). Numerous methodologies have been used to silence the corticothalamic projection, including pharmacological inactivation, ablation, and cooling of the visual cortex. The results of many of these studies are difficult to compare due to the differences in visual stimuli. Furthermore, some studies used ablation (e.g., Murphy and Sillito 1987), with which it is nearly impossible to collect data from the same LGN cell before and after inactivation of visual cortex.

During cortical cooling, we found a systematic reduction of the suppression elicited by high spatial frequency stimuli in LGN cells. Cooling never affected the responses of simultaneously recorded RGCs and also had no effect on the inhibition elicited in LGN cells by DC stimuli. Thus at the high spatial frequencies used in this study, the cortical input appears to be suppressive. We are unable to account for the great diversity in the results described by others. We did not observe a single instance where the cortical input appeared to be excitatory. We also never observed any phase change in the response of the cell during a cooling cycle, implying that the receptive fields did not move during cooling and that the phase of the response was not affected by inactivation of visual cortex.

The combined effects of RGCs and cortical feedback account for 78% of the suppression at high spatial frequencies observed in our population of LGN X-cells. Approximately half of the suppression observed at high spatial frequencies and half of the inhibition observed for spatially homogeneous (DC) stimuli in LGN cells are already present in the retinal input. Sources of the remaining suppression at high spatial frequencies and the remaining inhibition at DC are unknown. Possible sources are the local networks limited to the LGN (e.g., interneurons) and recurrent connections with the thalamic reticular nucleus.

### *Spatial extent*

Surround suppression that is not attributable to the classical surround has been referred to as the “extra classical receptive field” (Alitto and Usrey 2003; Solomon et al. 2006; Webb et al. 2002), “extra classical inhibition” (Solomon et al. 2002), and, most recently, as arising from a “suppressive field” (Bonin et al. 2005). The term “extra” has taken on multiple meanings, from the region located beyond the classical receptive field to simply a reduction of the

response elicited by a stimulus confined to the center that is not attributable to the inhibitory classical surround. We show here that suppression by gratings whose spatial frequencies exceed that to which the classical surround responds is colocalized with the classical surround. This is in agreement with the work of Bonin et al. (2005) who show that this is also true for low spatial frequencies. A possible exception to this colocalization principle is the periphery effect (McIlwain 1964), modulation from remote visual field stimulation, found in the retina and LGN of cats (Fischer and Kruger 1974; Kruger and Fischer 1973; McIlwain 1964), and, to a lesser degree, in primates (Kruger 1977; Kruger et al. 1975; Solomon et al. 2006). The periphery effect is predominantly found in cells that respond transiently and with short latencies: Y-cells in the cat retina and LGN (Cleland et al. 1971; Ikeda and Wright 1972; McIlwain 1964) and M-cells in the primate (Kruger 1977; Solomon et al. 2006).

#### *Gain control*

High spatial frequency gratings in the surround of LGN cells reduced the gain of stimuli limited to the receptive field center. The suppressive action of high spatial frequency gratings appears to reduce the gain in a complex manner, likely a combination of response gain control and contrast gain control. However, the cortical component of the suppression elicits a change in  $R_{\max}$  alone and therefore acts only as a response gain control (Heeger 1992). Solomon et al. (2002) also found that high spatial frequency stimuli in an annular grating placed beyond the classical receptive field divisively reduced responses elicited from the classical receptive field, but they did not inactivate cortex. Webb et al. (2002) found no effect of cortical ablation on the gain of the classical receptive field, but their stimuli were limited to the optimal spatial frequency and responses of the same cells were not recorded before and after ablation.

Our results are in essential agreement with Bonin et al. (2005), although they did not inactivate cortex and did not allow for feedback contributions such as those that we have identified. They observed suppression at spatial frequencies above those to which the classical surround is responsive and our data suggest that this suppression arises from both feed-forward and feedback mechanisms.

Our observations are not in agreement with those of Przybyszewski et al. (2000). They observed diminished responses from LGN cells during cortical inactivation and suggested that the visual cortex multiplicatively enhances responses in the primate LGN.

We cannot account for this discrepancy. The stimulus used by Przybyszewski et al. (2000) may not have encompassed the entire classical receptive field, although we did not see a single instance of decreased LGN responses at any stimulus size during cooling. It seems unlikely that it can be accounted for by species differences, although we cannot rule out this possibility.

#### *Orientation selectivity*

We found that suppression of LGN X-cell responses by high spatial frequencies was independent of the relative orientation

of the center and surround gratings. This is diametrically opposed to the findings of Cudeiro and Sillito (1996) who described stronger suppression when the center and annular gratings were iso-oriented than when they were orthogonal. Our methodologies appear similar, although they argued that this differential suppression was more evident at low spatial frequencies. However, recent studies in cat and primate (Bonin et al. 2005; Solomon et al. 2002; Webb et al. 2002) also failed to find any effect of relative orientation at any spatial frequency. For the moment, no obvious explanation for this discrepancy presents itself.

#### *Extending the DOG model*

We show that the peak and cutoff spatial frequencies obtained experimentally are lower than those derived from the DOG model. In many studies, spatial frequency tuning curves have been fit with a DOG function and the extracted parameters used to establish the characteristics of the center and surround of the classical receptive field (e.g., Enroth-Cugell et al. 1983). Our results show that spatial frequency tuning curves include suppression at high spatial frequencies that is not accounted for by the DOG model, thus calling into question the validity of fitting spatial frequency tuning curves with a DOG function.

Bonin et al. (2005) proposed a model for RGC and LGN cell receptive fields that combines the classical DOG mechanism with a suppressive field that includes a Gaussian-weighted bank of filters. This model has been shown to account for many aspects of RGC and LGN cell receptive fields. The authors suggested that the nonlinear component of the receptive field is suppressive at all spatial frequencies. As a result, the spatial summation curves collected using a spatially homogeneous stimulus would overestimate the strength and underestimate the size of the classical surround. This suggests that the classical surround is weaker and larger than we predicted and therefore the peak of the predicted curve in Fig. 11A would shift to lower frequencies, more closely matching the measured spatial frequency tuning curve. However, the cutoff of the predicted tuning curve would not be affected by a weaker and larger classical surround because the classical surround is not tuned to high spatial frequencies. The differences in measured and predicted cutoffs, although small, suggest that the role of suppression at high spatial frequencies is to restrict the response to large stimuli of high spatial frequencies.

Bonin et al. (2005) also showed that the action of the suppressive field is stronger at low spatial frequencies and high temporal frequencies, both incommensurate with cells in visual cortex, and therefore suggest that the suppressive field does not contain a cortical component. Our findings show that a cortical contribution to the suppressive field must be integrated into the model because cortical feedback modulates the gain of LGN relay cells, thereby contributing to the reduced response observed when receptive fields are stimulated with high spatial frequency gratings in the surround.

#### *Circuitry*

It is well established that outputs from layer VI of visual cortex make both direct, excitatory glutamatergic synapses

on the distal dendrites of LGN relay cells and indirect, inhibitory connections by way of the thalamic reticular nucleus (TRN) (Ahlsen et al. 1982; Descheenes and Hu 1990; Montero 1989, 1990; Robson 1983). Weak excitatory influences of this cortical input have been inferred in several experiments (Baker and Malpeli 1977; Funke et al. 1996; Hull 1968; Kalil and Chase 1970; Przybyszewski et al. 2000; Waleszczyk et al. 2005; Worgotter et al. 1998), including decreased spontaneous activity during cortical inactivation (Marrocco et al. 1996; Waleszczyk et al. 2005). We found no evidence for an excitatory effect of cortical inputs to LGN X-cells and, as observed by Przybyszewski et al. (2000) and Webb et al. (2002), we found spontaneous activity to be unchanged during cortical cooling.

We found that suppression by high spatial frequency gratings was diminished during cortical inactivation. This inhibitory effect of cortical input to the LGN is probably mediated by indirect action through the TRN. It is noteworthy that Golshani et al. (2001) found that the cortical input to the TRN is stronger than the cortical input to LGN relay neurons, suggesting that the indirect inhibitory input to the LGN may exert more influence on the responses of LGN cells than the direct excitatory input. It is also likely that the suppression not accounted for by either feedforward retinal input or feedback from the cortex is mediated by recurrent inhibition through the TRN. We also note that our experiments were conducted under anesthesia and it is possible that other feedback effects could be observed in experiments conducted in the awake and behaving state. For example, experiments in awake animals may be required to demonstrate a functional role for the excitatory component of the corticothalamic projection. O'Connor et al. (2002) also showed that attention can modulate neural activity in the human LGN, presenting another possibility for the role of the corticothalamic projection that could be tested only in an awake animal.

#### ACKNOWLEDGMENTS

We thank P. Schiller for use of the cooling plate and Peltier device.

#### GRANTS

This work was supported by National Eye Institute (NEI) Grant R01-EY-016430 and NEI Vision Training Grant T32-EY-007035.

#### REFERENCES

- Ahlsen G, Grant K, Lindstrom S. Monosynaptic excitation of principal cells in the lateral geniculate nucleus by corticofugal fibers. *Brain Res* 234: 454–458, 1982.
- Alitto HJ, Usrey WM. Corticothalamic feedback and sensory processing. *Curr Opin Neurobiol* 13: 440–445, 2003.
- Baker FH, Malpeli JG. Effects of cryogenic blockade of visual cortex on the responses of lateral geniculate neurons in the monkey. *Exp Brain Res* 29: 433–444, 1977.
- Barlow HB. Summation and inhibition in the frog's retina. *J Physiol* 119: 69–88, 1953.
- Bishop PO, Burke W, Davis R. Synapse discharge by single fibre in mammalian visual system. *Nature* 182: 728–730, 1958.
- Bonin V, Mante V, Carandini M. The suppressive field of neurons in lateral geniculate nucleus. *J Neurosci* 25: 10844–10856, 2005.
- Cleland BG, Dubin MW, Levick WR. Sustained and transient neurones in the cat's retina and lateral geniculate nucleus. *J Physiol* 217: 473–496, 1971.
- Cleland BG, Lee BB, Vidyasagar TR. Response of neurons in the cat's lateral geniculate nucleus to moving bars of different length. *J Neurosci* 3: 108–116, 1983.
- Cudeiro J, Sillito AM. Spatial frequency tuning of orientation-discontinuity-sensitive corticofugal feedback to the cat lateral geniculate nucleus. *J Physiol* 490: 481–492, 1996.
- Descheenes M, Hu B. Electrophysiology and pharmacology of the corticothalamic input to lateral thalamic nuclei: an intracellular study in the cat. *Eur J Neurosci* 2: 140–152, 1990.
- Enroth-Cugell C, Robson JG, Schweitzer-Tong DE, Watson AB. Spatio-temporal interactions in cat retinal ganglion cells showing linear spatial summation. *J Physiol* 341: 279–307, 1983.
- Fischer B, Kruger J. The shift-effect in the cat's lateral geniculate neurons. *Exp Brain Res* 21: 225–227, 1974.
- Freygang WH Jr. An analysis of extracellular potentials from single neurons in the lateral geniculate nucleus of the cat. *J Gen Physiol* 41: 543–564, 1958.
- Funke K, Nelle E, Li B, Worgotter F. Corticofugal feedback improves the timing of retino-geniculate signal transmission. *Neuroreport* 7: 2130–2134, 1996.
- Golshani P, Liu XB, Jones EG. Differences in quantal amplitude reflect GluR4-subunit number at corticothalamic synapses on two populations of thalamic neurons. *Proc Natl Acad Sci USA* 98: 4172–4177, 2001.
- Heeger DJ. Normalization of cell responses in cat striate cortex. *Vis Neurosci* 9: 181–197, 1992.
- Hubel DH, Wiesel TN. Integrative action in the cat's lateral geniculate body. *J Physiol* 155: 385–398, 1961.
- Hull EM. Corticofugal influence in the macaque lateral geniculate nucleus. *Vision Res* 8: 1285–1298, 1968.
- Ikeda H, Wright MJ. Functional organization of the periphery effect in retinal ganglion cells. *Vision Res* 12: 1857–1879, 1972.
- Jones JP, Palmer LA. The two-dimensional spatial structure of simple receptive fields in cat striate cortex. *J Neurophysiol* 58: 1187–1211, 1987.
- Kalil RE, Chase R. Corticofugal influence on activity of lateral geniculate neurons in the cat. *J Neurophysiol* 33: 459–474, 1970.
- Kaplan E, Shapley R. The origin of the S (slow) potential in the mammalian lateral geniculate nucleus. *Exp Brain Res* 55: 111–116, 1984.
- Kruger J. Stimulus dependent colour specificity of monkey lateral geniculate neurones. *Exp Brain Res* 30: 297–311, 1977.
- Kruger J, Fischer B. Strong periphery effect in cat retinal ganglion cells. Excitatory responses in ON- and OFF-center neurones to single grid displacements. *Exp Brain Res* 18: 316–318, 1973.
- Kruger J, Fischer B, Barth R. The shift-effect in retinal ganglion cells of the rhesus monkey. *Exp Brain Res* 23: 443–446, 1975.
- Kuffler SW. Discharge patterns and functional organization of mammalian retina. *J Neurophysiol* 16: 37–68, 1953.
- Levick WR, Cleland BG, Dubin MW. Lateral geniculate neurons of cat: retinal inputs and physiology. *Invest Ophthalmol* 11: 302–311, 1972.
- Lomber SG, Payne BR, Horel JA. The cryoloop: an adaptable reversible cooling deactivation method for behavioral or electrophysiological assessment of neural function. *J Neurosci Methods* 86: 179–194, 1999.
- Marrocco RT, McClurkin JW, Alkire MT. The influence of the visual cortex on the spatiotemporal response properties of lateral geniculate nucleus cells. *Brain Res* 737: 110–118, 1996.
- McIlwain JT. Receptive fields of optic tract axons and lateral geniculate cells: peripheral extent and barbiturate sensitivity. *J Neurophysiol* 27: 1154–1173, 1964.
- Montero VM. Ultrastructural identification of synaptic terminals from cortical axons and from collateral axons of geniculo-cortical relay cells in the perigeniculate nucleus of the cat. *Exp Brain Res* 75: 65–72, 1989.
- Montero VM. Quantitative immunogold analysis reveals high glutamate levels in synaptic terminals of retino-geniculate, cortico-geniculate, and geniculo-cortical axons in the cat. *Vis Neurosci* 4: 437–443, 1990.
- Murphy PC, Sillito AM. Corticofugal feedback influences the generation of length tuning in the visual pathway. *Nature* 329: 727–729, 1987.
- Nolt MJ, Kumbhani RD, Palmer LA. Contrast-dependent spatial summation in the lateral geniculate nucleus and retina of the cat. *J Neurophysiol* 92: 1708–1717, 2004.
- Nolt MJ, Kumbhani RD, Palmer LA. Visual processing in the lateral geniculate nucleus of the cat. Program No. 506.13. 2005 Abstract Viewer and Itinerary Planner. Washington, DC: Society for Neuroscience, 2005. Online.
- O'Connor DH, Fukui MM, Pinsk MA, Kastner S. Attention modulates responses in the human lateral geniculate nucleus. *Nat Neurosci* 5: 1203–1209, 2002.

- Przybyczewski AW, Gaska JP, Foote W, Pollen DA.** Striate cortex increases contrast gain of macaque LGN neurons. *Vis Neurosci* 17: 485–494, 2000.
- Reid RC, Victor JD, Shapley RM.** The use of m-sequences in the analysis of visual neurons: linear receptive field properties. *Vis Neurosci* 14: 1015–1027, 1997.
- Robson JA.** The morphology of corticofugal axons to the dorsal lateral geniculate nucleus in the cat. *J Comp Neurol* 216: 89–103, 1983.
- Rodiek RW.** Quantitative analysis of cat retinal ganglion cell response to visual stimuli. *Vision Res* 5: 583–601, 1965.
- Saul AB, Humphrey AL.** Spatial and temporal response properties of lagged and nonlagged cells in cat lateral geniculate nucleus. *J Neurophysiol* 64: 206–224, 1990.
- Sillito AM, Cudeiro J, Murphy PC.** Orientation sensitive elements in the corticofugal influence on centre-surround interactions in the dorsal lateral geniculate nucleus. *Exp Brain Res* 93: 6–16, 1993.
- So YT, Shapley R.** Spatial tuning of cells in and around lateral geniculate nucleus of the cat: X and Y relay cells and perigeniculate interneurons. *J Neurophysiol* 45: 107–120, 1981.
- Solomon SG, Lee BB, Sun H.** Suppressing surrounds and contrast gain in magnocellular-pathway retinal ganglion cells of macaque. *J Neurosci* 26: 8715–8726, 2006.
- Solomon SG, White AJR, Martin PR.** Extraclassical receptive field properties of parvocellular, magnocellular, and koniocellular cells in the primate lateral geniculate nucleus. *J Neurosci* 22: 338–349, 2002.
- Waleszczyk WJ, Bekisz M, Wrobel A.** Cortical modulation of neuronal activity in the cat's lateral geniculate and perigeniculate nuclei. *Exp Neurol* 196: 54–72, 2005.
- Webb BS, Tinsley CJ, Barraclough NE, Easton A, Parker A, Derrington AM.** Feedback from V1 and inhibition from beyond the classical receptive field modulates the responses of neurons in the primate lateral geniculate nucleus. *Vis Neurosci* 19: 583–592, 2002.
- Wolfe J, Palmer LA.** Temporal diversity in the lateral geniculate nucleus of cat. *Vis Neurosci* 15: 653–675, 1998.
- Worgotter F, Nelle E, Li B, Funke K.** The influence of corticofugal feedback on the temporal structure of visual responses of cat thalamic relay cells. *J Physiol* 509: 797–815, 1998.